Hindawi
International Journal of Corrosion
Volume 2018, Article ID 1604507, 7 pages
https://doi.org/10.1155/2018/1604507

Research Article

A Comparative Study of Hydrogen-Induced Cracking Resistances of API 5L B and X52MS Carbon Steels

Rodrigo Monzon Figueredo, Mariana Cristina de Oliveira, Leandro Jesus de Paula, Heloisa Andréa Acciari, and Eduardo Norberto Codaro

School of Engineering, São Paulo State University (UNESP), Guaratinguetá, SP, Brazil

Correspondence should be addressed to Heloisa Andréa Acciari; heloisa@feg.unesp.br

Received 8 January 2018; Revised 8 April 2018; Accepted 10 April 2018; Published 13 May 2018

Academic Editor: Ramana M. Pidaparti

Susceptibility to hydrogen-induced cracking of API 5L B and X52MS low-carbon steels in NACE 177-A, 177-B, and 284-B solutions has been investigated by the present work. A metallographic analysis of these steels was performed before and after NACE TM0284 standard testing. Corrosion products were characterized by scanning electron microscopy and X-ray dispersive energy spectrometry, which were subsequently identified by X-ray diffraction. Thus it was found that pH directly affects the solubility of corrosion products and hydrogen permeation. Both steels showed generalized corrosion in solution 177-A, and a discontinuous film was formed on their surfaces in solution 177-B; however, only the API 5L B steel failed the HIC test and exhibited greater crack length ratio in solution 177-A. In solution 284-B whose pH is higher, the steels exhibited thick mackinawite films with no internal cracking.

1. Introduction

In the latest decades, the world has been experiencing a continuous growth in the demand for oil and its derivatives. Despite all efforts to diversify the energy matrix world, current projections still reveal a considerable increase in the demand for oil and natural gas. This growing demand and the fact that many countries aim to obtain strategic autonomy from their energy matrix have led to increased exploitation complex oil and gas sources [1]. These sources present greater geological (depth, pressure, and temperature) and geographical (remote regions and marine currents) difficulties, as well as products with higher concentrations of hydrogen sulfide, commonly known as sour gas. The corrosion of steel pipelines by hydrogen sulfide has been a recurrent problem for oil and natural gas exploitation and production industry, which has aroused special attention after the discovery of the Brazilian pre-salt in 2006. Hydrogen sulfide together with other characteristics of the medium, such as temperature and pH condition, can cause general corrosion, localized corrosion, embrittlement, and cracking of pipelines; moreover, there is a large history of such occurrences in valves and welded joints. Pipeline rupture or its parts also have great environmental and economic impacts due to leaks and explosions, which lead to a halt in production [2–5]. Although corrosion consequences are well known, causes and mechanisms by which each phenomenon occurs are still not well understood. General corrosion is attributed to the preferential dissolution of the ferritic phase and it often manifests by a cementite scale (Fe_3C) formation. Localized corrosion arises from the galvanic couples between the ferritic phase and nonmetallic (e.g., MnS) or intermetallic (e.g., Fe_3C) inclusions and it manifests as pitting [6, 7].

The steps of a possible mechanism of hydrogen-induced cracking (HIC) can be, first, interstitial diffusion of hydrogen atoms under the steel surface. It occurs at a rate that depends on the packaging of the iron unit cell, that is, greater diffusibility in the ferrite phase (bcc) than in the more compact austenite phase (fcc). Then, hydrogen concentration at trapping sites: punctiform defects (gaps), linear defects (dislocations), two-dimensional defects (grain contours, mainly triple grain junction), and discontinuities (pores and contours of intermetallic particles such as Fe_3C, nonmetallic inclusions such as MnS, and impurities as oxides). The next step can be

Table 1: Chemical composition of API 5L X52MS and API 5L B steels (wt.%).

Steel	C	Si	Mn	P	S	V	Nb	Ti
X52MS	0.03	0.21	1.18	0.01	0.000	0.004	0.03	0.01
B	0.10	0.32	0.86	0.02	0.002	0.002	0.02	0.02

Table 2: Mechanical properties of steels.

Steel	FL (MPa)	RL (MPa)	EL (%)	Hardness (HV_{10})	Tenacity at −20°C (J)
X52MS	440	485	44	173	403
B	373	458	41	170	205

hydrogen atoms interaction with other atoms or cations in these sites of the iron crystalline network and hence decrease of the reticular energy (decohesion). After that, the recombination of hydrogen atoms and pressurization of these sites causes internal stress. Finally, this pressurization is manifested mainly in the form of blisters near the steel surface and internal cracks aligned in the direction of material rolling (HIC) [2, 8].

Since the chemical compositions of petroleum, natural gas, and produced water vary widely, and laboratory tests cannot reproduce the internal conditions of oil and gas pipelines, standard tests have been developed for qualifying of carbon steels. Corrosion standard tests of carbon steels to be used in oil and gas production establish specific conditions for pH, temperature, H_2S partial pressure, and time of exposure [8, 9]. It is important to note that the test solutions described by these standards do not simulate a sour environment but rather provide a reproducible test environment capable of evaluating the susceptibility to cracking of different steels in a relatively short period of time. In the pipe manufacturing industry, it is common to classify steels according to their corrosion resistance in one of these test solutions. However, there is always uncertainty in trying to extrapolate results based on production and test history, that is, how a product would behave in a low pH medium when it was originally designed and qualified for being used in a high pH medium.

Thus, the present work aims to study the resistance to hydrogen-induced cracking of API 5L B and X52MS steels in 177-A, 177-B, and 284-B NACE solutions. The corrosion products were characterized by electron microscopy (SEM) and X-ray dispersive energy spectrometry (EDS) and identified by X-ray diffraction (XRD).

2. Materials and Methods

API 5L X52MS and API 5L B carbon steels pipes are commonly manufactured in Brazil. The first one is produced to resist harsh sour conditions, whereas the last one is used in sweet or slightly acidic environments. The pipes were manufactured according to standard [10] through the cold forming process by three-stage pressing (edge pressing, U-shaped pressing, and O-shaped pressing), followed by longitudinal submerged arc welding, and expansion in order to calibrate the final geometry of pipes.

Table 3: Chemical composition of solutions 177-A and 177-B.

Compounds	Concentration (wt.%)	
	177-A	177-B
NaCl	5.0	5.0
HCH_3COO	0.50	2.5
$NaCH_3COO$	-	0.41

Chemical composition of these steels (Table 1) was determined by optical emission spectrometry with a Thermo ARL 3460 spectrometer and the ARL WinOE software.

The API 5L X52MS steel is quite able to support operation in H_2S-containing environments, being qualified in the manufacturing plant through tests in solution 177-A (Table 2). It should have maxima CLR (crack length ratio), CTR (crack thickness ratio), and CSR (crack sensitivity ratio) at 15%, 5.0%, and 2.0%, respectively, to be considered qualified [3]. The API 5L B steel used herein has not been heat-treated, thus not being appropriate for all the sour environments. It was chosen so as to compare hydrogen-induced cracking resistances of the two steels. Samples of 100 × 20 × 10 mm were taken from the pipes by plasma cutting at approximately 90 degrees from the longitudinal weld.

To evaluate their resistance to HIC, two flasks were used for each test, one containing 10 L of test solution (Tables 3 and 4) and the other one with 10 100 × 20 × 10 mm samples, being five of each steel (Figure 1). These samples were placed on a plastic grid at 25 mm from the bottom of the vessel being at least 15 mm apart from each other. A screwed cap and a rubber gasket ring closed the vessels. An inlet valve with a delivery tube was used for gas injection and solution test transferring. An outlet valve was used for internal pressure relief and gas washing. The vessels and gas-washing bottle were placed inside a laboratory fume hood equipped with a hydrogen sulfide detector. The test solution was purged of air with $N_{2(g)}$ 99.999% for 1 h at 100 mL/min per liter of test solution prior to transferring the test solution into the test vessel. Then, 8.0 L of test solutions was transferred by positive pressure of $N_{2(g)}$. The test vessel containing the test solution was purged with $N_{2(g)}$ for 1 h at 100 mL/min per liter of test solution and then saturated with $H_2S_{(g)}$ 99.9% at the same flow rate so as to ensure that the test solution

Table 4: Composition of solution 284-B adjusted to pH 8.2 with NaOH.

Compounds ($g\,L^{-1}$)	NaCl	Na_2SO_4	$MgCl_2{\cdot}6H_2O$	$CaCl_2$	$SrCl_2{\cdot}6H_2O$
	24.53	4.09	11.11	1.16	0.042
	KCl	$NaHCO_3$	KBr	H_3BO_3	NaF
	0.695	0.201	0.101	0.027	0.003

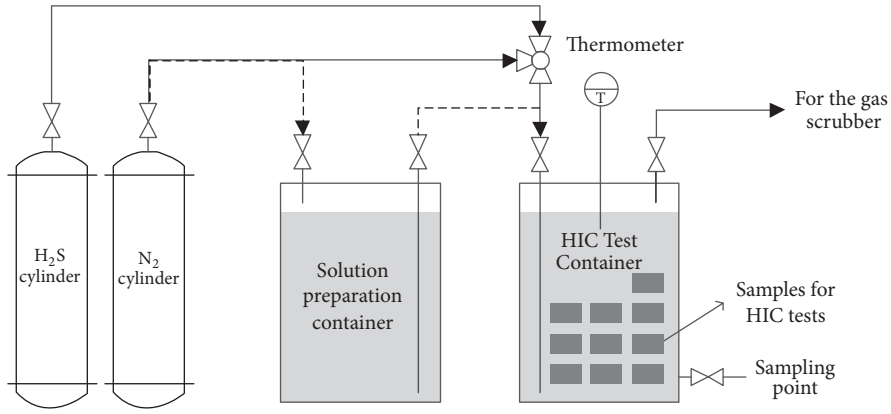

Figure 1: Hydrogen-induced cracking test apparatus.

remains saturated with $H_2S_{(g)}$ for 96 hours of testing. The tests were performed at a temperature of 24°C ± 3°C. At every 24 h, an aliquot of the test solution was collected in order to measure pH and $H_2S_{(g)}$ concentration, with the former being by iodometric titration. According to standard test method [8], the standard pH range for 177-A solution was 2.6 to 2.8 at the beginning of the test and <4.0 at the end of the test; for 177-B, the range was set at 3.4 to 3.6 at the beginning and <4.0 at the end; for 284-B the range is from 8.1 to 8.3 at the beginning and 4.8 to 5.4 at the end of the test. In this work, pH values and $H_2S_{(g)}$ concentrations (≥2,300 ppm) were in good agreement with the aforementioned NACE standard. After 96 h, the desulfurization process was initiated by bubbling with $N_{2(g)}$. The test vessel was drained and opened, and the samples were carefully washed in deionized water, dried under stream of $N_{2(g)}$, and introduced into a desiccator containing silica, which was connected to a vacuum pump.

Scanning electron microscopy (SEM) analyses were carried out on surfaces and cross sections of samples with a Jeol 6350 scanning electron microscope. Local chemical composition was determined by X-ray dispersive energy spectrometry (EDS) using a Thermo C10015 probe controlled by the Noran System SIX software. X-ray diffraction (XRD) analyses were carried out on corroded surfaces using the Bruker D8 Advance Eco diffractometer equipped with the DIFFRAC.EVA software. In order to study the temporal evolution of corrosion products in a longer immersion time, a further experiment was performed, thus exposing a new sample to solution 284-B for 35 days at room temperature. In this case, by following the preparation and transfer stages of solution 284-B, the test vessel containing the test solution was purged with $N_{2(g)}$ for 1 h at 100 mL/min per liter of 284-B and then saturated with $H_2S_{(g)}$ 99.9% for 1 h at the same flow rate (i.e., nonstationary conditions).

3. Results and Discussion

API 5L X52MS carbon steel shows the ferritic-bainitic matrix with high grain refinement and random inclusion distribution (Figure 2(a)). On the other hand, API 5L B carbon steel shows a ferrite-pearlite microstructure and presence of banding (Figure 2(b)).

Cross-sectional analyses of the API 5L X52MS samples have not revealed the occurrence of cracks in any of the test solutions (Table 5), which is probably due to a low concentration of alloying elements with subsequent low segregation and banding of the microstructure. The API 5L B samples obtained high values of CLR and CTR for solution 177-A, that is, 40% higher than those observed in solution 177-B on average, and no cracks were found in solution 284-B, as shown in Table 6.

These results are directly associated with hydrogen permeation throughout steel. The concentration of hydrogen ions decreases as the pH and deposited film thickness increase, which can hinder hydrogen diffusion and penetration into steel [6, 11]. Cracks can be observed in the cross sections of samples exposed to solutions 177-A and 177-B, respectively, in Figures 3 and 4.

SEM in Figure 5(a) shows cracks towards the same direction, that is, parallel to the sample surface. Figure 5(b) shows details of crack nucleation from the inclusion of MnS into steel B. Figure 5(c) shows the results of the EDS analysis of a region indicated by an arrow in Figure 5(b). Cracks were mainly developed during the elongated inclusions of MnS, as observed in Figure 5(b). The composition of the

Table 5: HIC test results for the API 5L X52MS steel.

177-A				177-B				284-B			
CP	CLR	CTR	CSR	CP	CLR	CTR	CSR	CP	CLR	CTR	CSR
1	0	0	0	7	0	0	0	12	0	0	0
2	0	0	0	8	0	0	0	13	0	0	0
3	0	0	0	9	0	0	0	14	0	0	0
4	0	0	0	10	0	0	0	15	0	0	0
5	0	0	0	11	0	0	0	16	0	0	0
Med	0	0	0	Med	0	0	0	Med	0	0	0

Table 6: HIC test results for the API 5L B steel.

177-A				177-B				284-B			
CP	CLR	CTR	CSR	CP	CLR	CTR	CSR	CP	CLR	CTR	CSR
16	26%	3%	1%	21	29%	3%	1%	26	0	0	0
17	35%	4%	1%	22	27%	3%	1%	27	0	0	0
18	48%	4%	2%	23	32%	4%	1%	28	0	0	0
19	35%	5%	2%	24	16%	2%	0%	29	0	0	0
20	46%	7%	3%	25	32%	1%	0%	30	0	0	0
Med	38%	5%	2%	Med	27%	2%	1%	Med	0	0	0

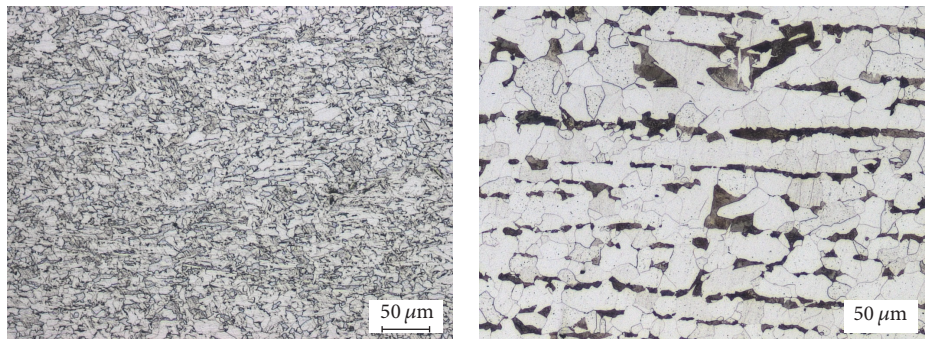

(a) (b)

Figure 2: Microstructure of the central region of the API 5L steel plates: (a) X52MS and (b) B (metallographic etchant: 3.0% nital solution).

Figure 3: Stepwise cracks in the cross section of the API 5L B sample exposed to solution 177-A.

Figure 4: Stepwise cracks in the cross section of the API 5L B sample exposed to solution 177-B.

inclusion at the crack tip in Figure 5(b) is presented in the EDS spectrum of Figure 5(c), in which S and Mn peaks can be clearly observed.

It is well known that the cracking in H_2S environments is associated with the presence of nonmetallic inclusions, such as MnS and Ti or V carbonitrides, and a banded structure. The heterogeneous distribution of these inclusions also favors cracking due to the higher concentration of hydrogen traps in some regions. Segregations associated with high levels of P and S in steel contribute to the accumulation of hydrogen in the material [7, 12–16].

The surface analysis has revealed that, for the lowest pH solution (177-A solution), there was no film formation on the sample, as shown in Figures 6(a) and 6(b) and confirmed by the EDS analysis of region 3, Figure 6(c), in which only peaks associated with Fe and Mn are observed. The carbon steel exhibited generalized corrosion at low pH, probably due to high solubility of iron sulfide and preferential attack of ferritic phase [6, 7]. In solution 177-B, a discontinuous layer with some degree of crystallinity was observed on a region of the surface shown in Figures 6(d) and 6(e). The EDS analysis

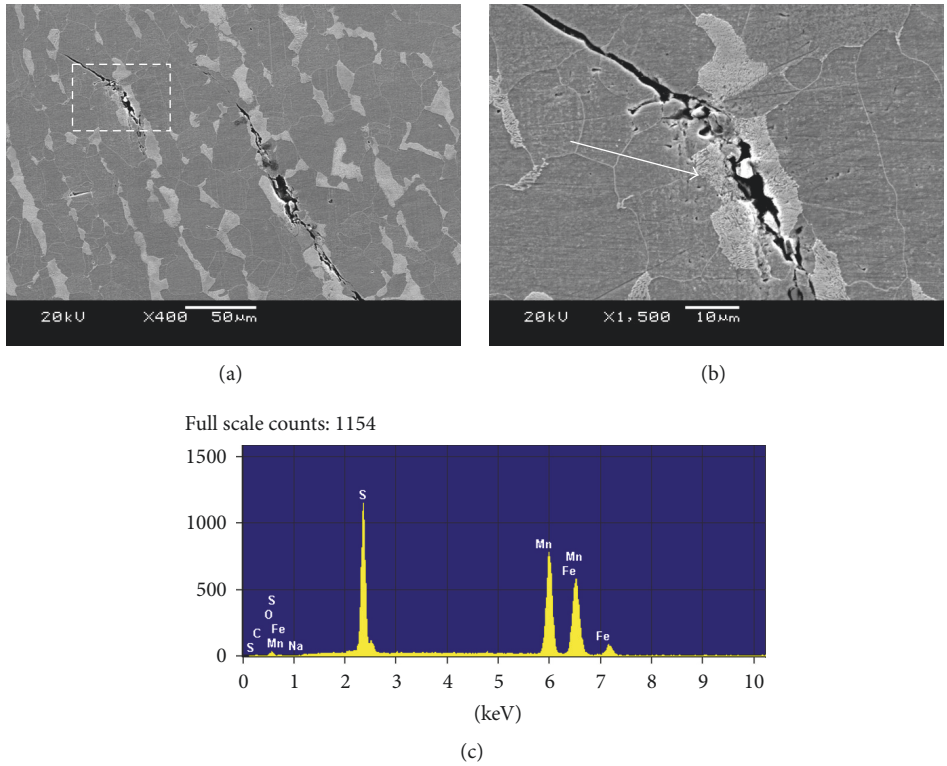

Figure 5: Micrographs showing details of crack nucleation from the inclusion of MnS into the API 5L B steel: (a) 400x and (b) 1500x; (c) EDS analysis of the region indicated by an arrow at (b) micrograph.

indicates sulfur-rich sulfides (nonstoichiometric FeS) in the crystalline region depicted in Figure 6(f). Similar surface characteristics were reported in another work on low-carbon steels in 5.0% NaCl solution saturated with H_2S and pH 4.2 [17]. It was not possible to identify any iron sulfides by the XRD analysis due to a small amount of corrosion products.

In solution 284-B at a higher pH, there was a considerable amount of insoluble sulfides resulting from the saturation step with H_2S, as shown in Figures 6(g) and 6(h) and confirmed by the EDS of region 3 in Figure 6(i). This thick film probably provides greater resistance to diffusion of ionic species, thus hindering the corrosion process in comparison with discontinuous films formed at a lower pH. The XRD surface analysis has only identified corrosion products formed in solution 284-B. The diffractogram of corrosion products obtained after 96 h of exposure (Figure 7) shows peaks at approximately 18°, 30°, 35°, 38°, 50°, and 54° which are the same as those of mackinawite (M), that is, a tetragonal crystalline form of iron sulfide [18]. A similar diffractogram has been reported by Zheng et al. [19] and Zhou et al. [20].

Several iron sulfide polymorphs have been identified within oil and gas pipelines. The most cited monosulfides are tetragonal mackinawite, hexagonal troilite, monoclinic pyrrhotite, and hexagonal pyrrhotite, all which are relatively stable in oxygen-free acid media [21–23]. Corrosion tests at room temperature using artificial sea water or any other salt solutions saturated with hydrogen sulfide often lead to one or two types of iron sulfides, that is, mackinawite (kinetically favored product) and pyrrhotite (thermodynamically favored product).

In order to study the temporal evolution of corrosion products, another corrosion test was performed in a longer immersion time in solution 284-B. The diffractogram of corrosion products obtained after 35 days of exposure only showed mackinawite peaks (Figure 8). When compared to Figure 7, mackinawite peaks increase and iron peaks decrease, which is probably due to surface coverage and the sulfide layer thickening during immersion time.

4. Conclusion

Cracking resistance seems to be directly associated with the steel microstructure and medium acidity. API 5L B and X52MS steels showed generalized corrosion in solution 177-A. Both steels formed a discontinuous layer when exposed to solution 177-B. Only the API 5L B steel failed the HIC test and exhibited a larger crack length ratio in solution 177-A. The SEM-EDS analysis reveals that cracks were initiated in the MnS inclusions. In solution 284-B, a thick mackinawite film was formed on both steels, and no crack in their microstructures was observed. When the API 5L X52MS steel was exposed to a longer immersion time, mackinawite was the only corrosion product obtained from the process.

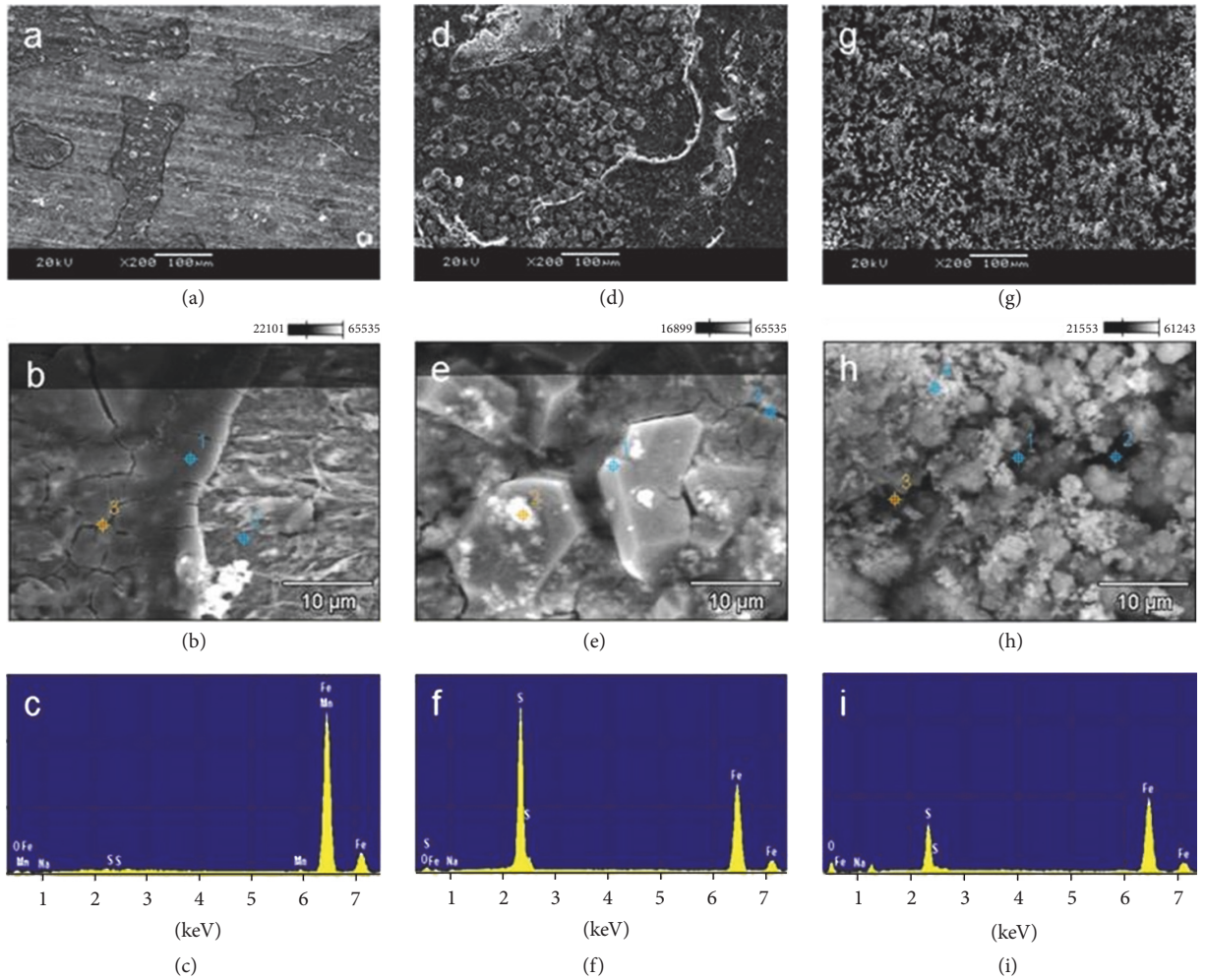

Figure 6: SEM and EDS analyses of corrosion products in the API 5L X52MS steel. This steel exposed to 177-A solution: (a) 200x, (b) 3000x, and (c) EDS. This one exposed to 177-B solution: (d) 200x, (e) 3000x, and (f) EDS. This one exposed to 284-B solution: (g) 200x, (h) 3000x, and (i) EDS.

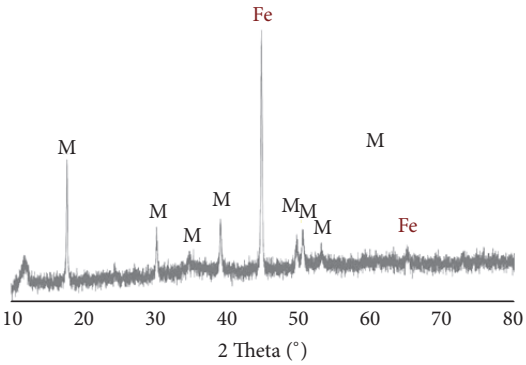

Figure 7: XRD analysis of the API 5L X52MS steel exposed to solution 284-B for 96 h (M: mackinawite).

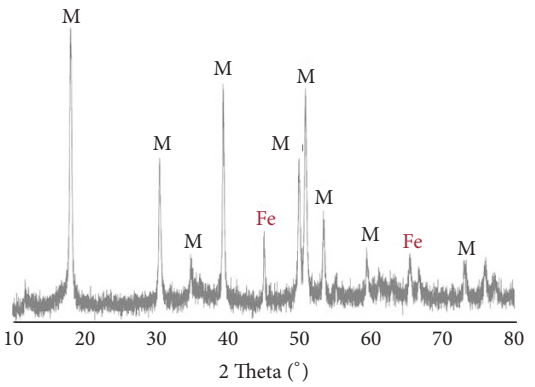

Figure 8: XRD analysis of the API 5L X52MS steel exposed to solution 284-B for 35 days (M: mackinawite).

Data Availability

The data used to support the findings of this study are available from the corresponding author upon request.

Conflicts of Interest

The authors declare that they have no conflicts of interest.

Acknowledgments

The authors would like to thank PROEX/UNESP, CAPES, and FAPESP (Process 2017/11361-5) for the financial support.

References

[1] IEA, *Resources to Reserves 2013 - Oil, Gas and Coal Technologies for the Energy Markets of the Future*, International Energy Agency, Paris, France.

[2] M. A. Mohtadi-Bonab, J. A. Szpunar, R. Basu, and M. Eskandari, "The mechanism of failure by hydrogen induced cracking in an acidic environment for API 5L X70 pipeline steel," *International Journal of Hydrogen Energy*, vol. 40, no. 2, pp. 1096–1107, 2015.

[3] ISO, "Petroleum and Natural Gas Industries - Materials for use in H_2S-Containing Environments in Oil and Gas Production - Part 1," Tech. Rep. ISO 15156-1, International Organization for Standardization, Switzerland, 2009.

[4] D. Talbot, *Corrosion Science and Technology*, CRC Press, New York, NY, USA, 2007.

[5] B. P. Tissot and D. H. Welte, *Petroleum Formation and Occurrence*, Springer, Berlin, Germany, 2nd edition, 1984.

[6] C. Zhou, S. Zheng, C. Chen, and G. Lu, "The effect of the partial pressure of H2S on the permeation of hydrogen in low carbon pipeline steel," *Corrosion Science*, vol. 67, pp. 184–192, 2013.

[7] J. Sojka, M. Jérôme, M. Sozańska, P. Váňová, L. Rytířová, and P. Jonšta, "Role of microstructure and testing conditions in sulphide stress cracking of X52 and X60 API steels," *Materials Science and Engineering: A Structural Materials: Properties, Microstructure and Processing*, vol. 480, no. 1-2, pp. 237–243, 2008.

[8] NACE International, "Evaluation of Pipeline and pressure vessel steel for resistance to hydrogen-induced crack," Tech. Rep. ANSI/NACE TM0284, NACE International, Houston, Tex, USA, 2017.

[9] NACE International, "Standard test method laboratory testing of metals for resistance to sulfide stress cracking and stress corrosion cracking in H_2S environments," Tech. Rep. ANSI/NACE TM0177, NACE International, Houston, Tex, USA, 2016.

[10] API 5L, "Specification for Line Pipe," Tech. Rep., API Publishing Services, Washington, Wash, USA, 2012.

[11] K. Kobayashi, T. Omura, M. Okatsu, T. Hara, and N. Ishikawa, "Proposal of HIC test solution with buffer capacity in NACE TM0284," in *Proceedings of the NACE - International Corrosion Conference Series*, Orlando, Fla, USA, 2013.

[12] F. Huang, J. Liu, Z. Deng, J. Cheng, Z. Lu, and X. Li, "Effect of microstructure and inclusions on hydrogen induced cracking susceptibility and hydrogen trapping efficiency of X120 pipeline steel," *Materials Science and Engineering: A Structural Materials: Properties, Microstructure and Processing*, vol. 527, no. 26, pp. 6997–7001, 2010.

[13] L. Gan, F. Huang, X. Zhao, J. Liu, and Y. F. Cheng, "Hydrogen trapping and hydrogen induced cracking of welded X100 pipeline steel in H_2S environments," *International Journal of Hydrogen Energy*, vol. 43, no. 4, pp. 2293–2306, 2018.

[14] M. Elboujdaini and R. W. Revie, "Metallurgical factors in stress corrosion cracking (SCC) and hydrogen-induced cracking (HIC)," *Journal of Solid State Electrochemistry*, vol. 13, no. 7, pp. 1091–1099, 2009.

[15] A. C. Palmer and R. A. King, *Subsea Pipeline Engineering*, PennWell, Tulsa, Okla, USA, 2008, Subsea Pipeline Engineering.

[16] M. A. Mohtadi-Bonab and M. Eskandari, "A focus on different factors affecting hydrogen induced cracking in oil and natural gas pipeline steel," *Engineering Failure Analysis*, vol. 79, pp. 351–360, 2017.

[17] P. Bai, S. Zheng, and C. Chen, "Electrochemical characteristics of the early corrosion stages of API X52 steel exposed to H_2S environments," *Materials Chemistry and Physics*, vol. 149, pp. 295–301, 2015.

[18] J. Ning, Y. Zheng, B. Brown, D. Young, and S. Nesic, "Construction and verification of pourbaix diagrams for hydrogen sulfide corrosion of mild steel," in *Proceedings of the NACE - International Corrosion Conference Series*, Dallas, Tex, USA, 2015.

[19] S. Zheng, C. Zhou, X. Chen, L. Zhang, J. Zheng, and Y. Zhao, "Dependence of the abnormal protective property on the corrosion product film formed on H2S-adjacent API-X52 pipeline steel," *International Journal of Hydrogen Energy*, vol. 39, no. 25, pp. 13919–13925, 2014.

[20] C. Zhou, X. Chen, Z. Wang, S. Zheng, X. Li, and L. Zhang, "Effects of environmental conditions on hydrogen permeation of X52 pipeline steel exposed to high H_2S-containing solutions," *Corrosion Science*, vol. 89, no. C, pp. 30–37, 2014.

[21] S. N. Smith, B. Brown, and W. Sun, "Paper 11081 of NACE International," in *Proceedings of the Paper 11081 of NACE International*, Houston, Tex, USA, 2011.

[22] B. Craig, "Corrosion product analysis - a road map to corrosion in oil and gas production," *Materials Performance*, vol. 41, no. 8, pp. 56–58, 2002.

[23] S. N. Smith, "Corrosion product analysis in oil and gas pipelines," *Materials Performance*, vol. 42, no. 8, pp. 44–47, 2003.